OPEN

Journal of Cerebral Blood Flow & Metabolism (2015) 35, 521–526

www.jcbfm.com

ORIGINAL ARTICLE

Evaluation of cerebrovascular impedance and wave reflection in mouse by ultrasound

Christopher K Macgowan[1,2], Sarah Joy Stoops[2], Yu-Qing Zhou[3], Lindsay S Cahill[3] and John G Sled[1,3]

Genetic and surgical mouse models are commonly used to study cerebrovascular disease, but their size makes invasive hemodynamic testing technically challenging. The purpose of this study was to demonstrate a noninvasive measurement of cerebrovascular impedance and wave reflection in mice using high-frequency ultrasound in the left common carotid artery (LCCA), and to examine whether microvascular changes associated with hypercapnia could be detected with such an approach. Ten mice (C57BL/6J) were studied using a high-frequency ultrasound system (40 MHz). Lumen area and blood flow waveforms were obtained from the LCCA and used to calculate pulse-wave velocity, input impedance, and reflection amplitude and transit time under both normocapnic and hypercapnic (5% CO_2) ventilation. With hypercapnia, vascular resistance was observed to decrease by 87% ± 12%. Although the modulus of input impedance was unchanged with hypercapnia, a phase decrease indicative of increased total arterial compliance was observed at low harmonics together with an increased reflection coefficient in both the time (0.57 ± 0.08 versus 0.68 ± 0.08, $P = 0.04$) and frequency domains (0.62 ± 0.08 versus 0.73 ± 0.06, $P = 0.02$). Interestingly, the majority of LCCA blood flow was found to pass into the internal carotid artery (range = 76% to 90%, $N = 3$), suggesting that hemodynamic measurements in this vessel are a good metric for intracerebral reactivity in mouse.

Journal of Cerebral Blood Flow & Metabolism (2015) **35,** 521–526; doi:10.1038/jcbfm.2014.229; published online 17 December 2014

Keywords: cerebrovascular reactivity; hypercapnia; impedance; mice; reflection; ultrasound

INTRODUCTION

Under normal physiological conditions, the cerebral microvasculature has a large capacity to dilate or constrict in response to changing metabolic demand and changes in cardiac output. However, cerebral blood flow autoregulation can be impaired by a wide variety of pathological conditions including atherosclerosis, stroke, sickle cell anemia, syncope, traumatic brain injury, and Alzheimer's disease.[1–6] Impaired autoregulation is assessed clinically by measurement of cerebrovascular resistance or impedance, normally derived from direct catheter measurements of pressure and flow in a major artery.[7–10] Early work using catheter measurements suggested that increased reflections could be a biomarker of microcirculatory abnormalities; however, the invasiveness of catheterization has limited the broad application of this approach. Transcranial ultrasound provides a noninvasive alternative for studying cerebrovascular reactivity, based on changes in the Doppler waveform of central cerebral blood vessels such as the middle cerebral artery. This idea that blood flow pulsatility provides an indirect measure of microvascular impedance is well accepted, for instance in the context of transcranial ultrasound assessment of late-gestation at-risk fetuses.[11] Unfortunately, such an approach requires an acoustic window to the target vessel, and failure rates of 25% have been reported in adults, where the mature skull is a barrier to access.[12] There is potential, however, to infer the characteristics of the cerebral microcirculation based on the pulsation characteristics of the common carotid artery (CCA). Methods to do so generally rely on measurement of blood flow using Doppler ultrasound and estimates of blood pressure based on either surface measurements of arterial pulsation (tonometry) or imaging measurements of lumen area pulsation.[4,13–15]

In the present work, high-frequency ultrasound is used to study vascular impedance and wave reflection in mice noninvasively. Mice offer an advantage for such research in that genetically identical individuals may be raised and manipulated under controlled conditions, as done here. Furthermore, the growing list of genetically and experimentally induced mouse models of cerebrovascular disorders provides immediate applications for this technology in basic research studies.[16–18] Previous work by others in this area has described pressure wave propagation velocity (pulse-wave velocity (PWV)) and wave reflection by ultrasound in the carotid arteries of experimental mice,[19,20] but has not specifically examined whether microvascular changes can be detected with this approach. Here we present a method for assessing input impedance and wave reflection in the mouse CCA, and evaluate whether these measurements were sensitive to changes in cerebral microvascular tone induced by hypercapnia.

MATERIALS AND METHODS

Animals

Ten male C57BL/6J mice from the Jackson Laboratory (Bar Harbor, ME, USA) were studied at 12 weeks of age (mean ± s.d. body weight of 26.5 ± 1.9 g). All animal experiments were approved by the Animal Care

[1]Department of Medical Biophysics, University of Toronto, Toronto, Ontario, Canada; [2]Division of Physiology and Experimental Medicine, Hospital for Sick Children, Peter Gilgan Centre for Research and Learning, Toronto, Ontario, Canada and [3]Mouse Imaging Centre, The Hospital for Sick Children, Peter Gilgan Centre for Research and Learning, Toronto, Ontario, Canada. Correspondence: Dr CK Macgowan, Division of Physiology and Experimental Medicine, Hospital for Sick Children, Peter Gilgan Centre for Research and Learning, Room 08.9714, 686 Bay Street, Toronto, ON M5G 0A4, Canada.
E-mail: Christopher.Macgowan@sickkids.ca
This study was funded by the Canadian Institutes of Health Research Grant MPI-199854.
Received 19 August 2014; revised 14 November 2014; accepted 25 November 2014; published online 17 December 2014

Committee at the Toronto Centre for Phenogenomics, following the Canadian Council on Animal Care guidelines and the Animal Research: Reporting of *In Vivo* Experiments (ARRIVE) guidelines.

Animal Preparation

Mice were anesthetized with isoflurane (4% for induction; 1% for maintenance) and then endotracheally intubated (22 gauge catheter), placed supine on a temperature-regulated platform and mechanically ventilated using a pressure-controlled ventilator (TOPO Small Animal Ventilator, Kent Scientific, Torrington, CT, USA). The same ventilation parameters were used for all of the mice in the study (135 cycles per minute). In addition, 0.2 mg/kg pancuronium bromide (Sigma-Aldrich, St Louis, MO, USA) was injected intraperitoneally for muscle relaxation, ensuring optimal breathing control throughout the experiment. Hair from the throat and chest was removed using Nair (Church & Dwight Co., Inc., Ewing, NJ, USA) to improve contact with the ultrasound transducer. During ultrasound imaging, the body temperature was maintained at 36 to 37°C and the heart rate and respiration rate were continuously monitored.

Ultrasound Imaging

A high-frequency ultrasound imaging system (Vevo 2100, VisualSonics, Toronto, ON, Canada) with a 40 MHz linear array transducer was used (wavelength ~35 μm).[21] The M-mode trace and pulsed Doppler velocity spectrum were recorded from the left CCA, ~3 mm proximal to its bifurcation. M-mode recordings (pulse repetition rate = 1 kHz) were made with the ultrasound beam perpendicular to the left CCA, and pulsed Doppler velocity (pulse repetition rate = 15 to 25 kHz) was measured with the sample volume adjusted to cover the entire vascular lumen and the smallest intercept angle possible ($< 60°$) between the flow direction and the ultrasound beam. Diameter and flow velocity measurements were recorded while the mice inhaled a gas mixture of 30% O_2/70% N_2 (normocapnia) and were repeated after the gas mixture was changed to 5% CO_2, 30% O_2, balance N_2 (hypercapnia), a paradigm based on human studies of cerebrovascular reserve[22] (30% O_2 was necessary to prevent spontaneous gasping in mice during hypercapnia). The mice were exposed to the hypercapnic gas mixture for 5 minutes before the diameter and flow velocity measurements were acquired. This protocol was validated in a separate series of mice ($N = 22$) while monitoring pCO_2 levels transcutaneously (TCM4, Radiometer Canada, London, ON, Canada) and produced pCO_2 values (mean ± s.e.) in the two gas conditions of 35.5 ± 2.3 mm Hg and 53.5 ± 3.5 mm Hg, respectively.

Image Processing

M-mode and Doppler data were analyzed offline using automated routines developed in commercial software (Matlab—Mathworks, Natick, MA, USA). Vessel diameter was extracted from the M-mode data by automatically tracing the near and far wall positions, based on peak wall intensity. To avoid assumptions about the velocity profile, the spatial mean velocity (angle corrected) was quantified as the instantaneous centroid of the Doppler velocity spectrum, calculated using values between a manually specified lower bound and the maximum velocity envelope. Each waveform was then divided into cardiac cycles based on the recorded electrocardiogram. These area or velocity waveforms for individual cardiac cycles were truncated to have uniform length and averaged together. This produced consistent diameter and velocity waveforms, and provided an estimate of area and flow uncertainty. From the average waveforms, lumen area and flow volume versus time were calculated and used for subsequent impedance and reflection analysis.

Impedance and Reflection Analysis

Impedance and reflection estimates were obtained by passing the lumen area and flow waveforms through the following analysis pipeline.

First, the average area and flow waveforms were temporally aligned based on the timing of their initial upstroke (foot). The timing of the upstroke was established from the intersection of linear fits to the diastolic baseline and systolic rise of each waveform.[23] Next, the PWV was calculated based on the relative change in flow with respect to area during systole, a period assumed to be free of reflection.[24,25] Plotting flow versus area, a line was fit to the systolic portion using total least squares regression to account for uncertainty in both the area and flow estimates.[26] Through this process, linearity between area and flow during the systolic period was evaluated and used to refine the temporal alignment between the flow and area waveforms, on average by 0.5 ± 0.6 milliseconds. The flow waveforms were then decomposed into their forward and reflected components according to the following equations:[27–29]

$$q_+(t) = \frac{1}{2}[(q_m(t) + q_m(0)) + \mathrm{PWV}\cdot(a_m(t) - a_m(0))]$$
$$q_-(t) = \frac{1}{2}[(q_m(t) - q_m(0)) - \mathrm{PWV}\cdot(a_m(t) - a_m(0))] \quad (1)$$

where q_+ and q_- are the calculated forward and reflected flow waveforms, respectively, and q_m and a_m are the measured flow and area waveforms, respectively. Forward and reflected area waveforms were similarly calculated.

Wave transit time was defined as the delay between the onsets of q_+ and q_-. Transit time was then used in conjunction with PWV to estimate the distance to the nearest reflection site.

Reflection coefficients were calculated in both the time domain and frequency domain. The time domain reflection coefficient Γ_t was defined as the ratio of the peak-to-peak amplitudes of q_- and q_+. The frequency-domain definition of reflection was the conventional complex-valued parameter, $\Gamma(\omega)$, equal to the ratio of the frequency spectra of q_- and q_+. Here ω is in units of harmonics of the fundamental frequency. Frequency domain reflection was summarized as the magnitude of the reflection coefficient at the fundamental frequency, $|\Gamma(\omega = 1)|$.[8]

The input impedance, $Z_{in}(\omega)$, was calculated at nonzero frequencies using the following expression:

$$Z_{in}(\omega > 0) = \frac{\rho\cdot\mathrm{PWV}^2}{\bar{a}}\cdot\frac{A_m(\omega)}{Q_m(\omega)} \quad (2)$$

where ρ is the density of blood (1.06 g/mL), $\bar{a}$ is the average vessel area over the cardiac cycle, and $A_m(\omega)$ and $Q_m(\omega)$ are the frequency spectra of the measured area and flow waveforms, respectively.

Finally, the ratio of the systolic accelerations (i.e., upstroke slope) of q_+ and q_-, normalized by their peak-to-peak amplitudes, was used to quantify smoothing of the reflected wave relative to the forward wave.

Statistical Analysis

Statistical analysis was performed using R 3.0.2 (http://www.r-project.org/). Results were summarized as mean ± s.d. unless noted otherwise. Unmasked testing for population differences between the control and hypercapnia groups was performed using a paired *t*-test (two tailed). Statistical significance was defined as $P \leq 0.05$. Table data is reported as mean ± s.d. Figure error bars show s.e.

RESULTS

Representative ultrasound data from the left CCA of one mouse are presented in Figure 1, demonstrating the extraction of velocity and diameter waveforms with high precision and reproducibility from the source images. Although ultrasound image quality was good in all mice, 2 of the 10 mice had poorly defined ECG traces, which led to artifactually high variance in the flow and area waveforms between consecutive cardiac cycles. These two mice were thus excluded from subsequent analysis.

A summary of the hemodynamic variables measured under each gas condition is presented in Table 1. Relative to control conditions, heart rate was elevated during hypercapnia. Similarly, mean velocity and mean flow both increased with hypercapnia, whereas mean vessel area, a metric for mean pressure, showed a nonsignificant trend for higher values. Based on the flow and area changes, vascular resistance decreased with hypercapnia to 87% ± 12% of its baseline value.

Figure 2 demonstrates decomposition of a flow waveform into its forward and reflected components using the experimental flow and area data from Figure 1. Pulse-wave velocity is estimated first, based on the change in flow versus area (Figure 2A). The waveforms were then scaled, their baselines subtracted (Figure 2B), and the forward and reflected waveforms were calculated using equation (1). The resulting forward and reflected waveforms for these representative data are presented in Figure 2C. Quantitative

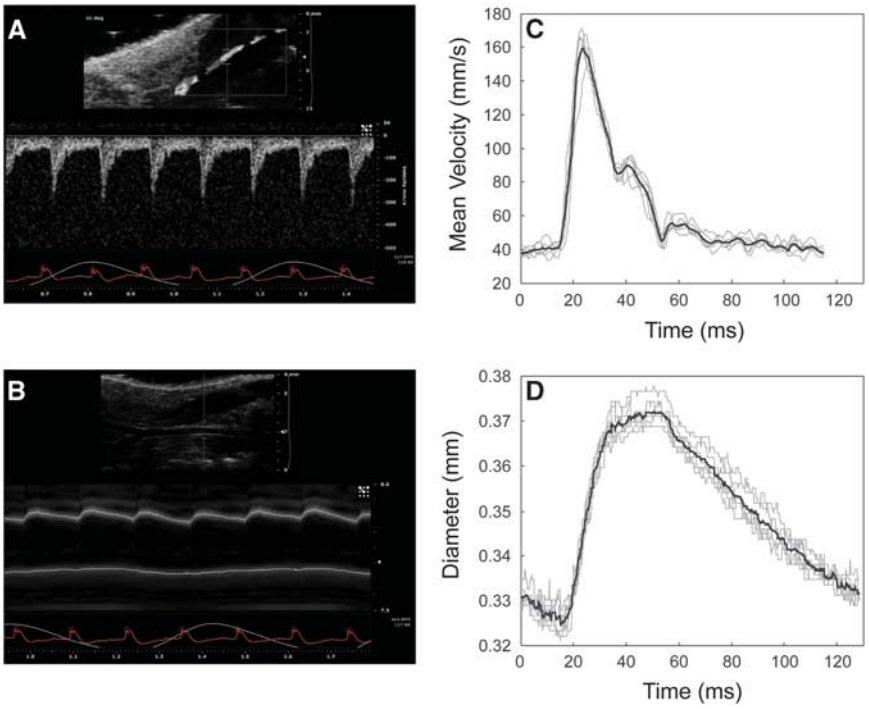

Figure 1. Measurement of blood velocity and lumen diameter in the left common carotid artery of mouse. (**A**) B-mode image used to prescribe the Doppler sample volume and corresponding spectral Doppler waveform. (**B**) B-mode image used to prescribe the M-mode scan, and the corresponding M-mode waveform. Superimposed on the Doppler spectra and the M-mode data are the mean velocity and wall position traces, respectively (white lines). Electrocardiography (red lines) and respiratory waveforms (yellow lines) are also shown, the former used to segment individual cardiac cycles. (**C** and **D**) Segmented diameter and velocity waveforms, respectively. Gray lines represent data from consecutive cardiac cycles and the black line represents their average.

Table 1. Heart rate, lumen area, blood velocity, and blood flow under nomocapnia and hypercapnia

	Control (mean ± s.d.)	*Hypercapnia (mean ± s.d.)*	P	*Absolute change (mean ± s.d.)*	*% change (mean)*
Heart rate (b.p.m)	508 ± 37	548 ± 28	0.05	39 ± 46	8%
Area (mm^2)	0.14 ± 0.05	0.18 ± 0.01	0.09	0.04 ± 0.05	35%
Mean velocity (cm/s)	8.8 ± 2.1	10.2 ± 2.3	0.03	1.5 ± 1.5	18%
Mean flow (cm^3/min)	0.8 ± 0.3	1.1 ± 0.3	0.01	0.3 ± 0.3	59%

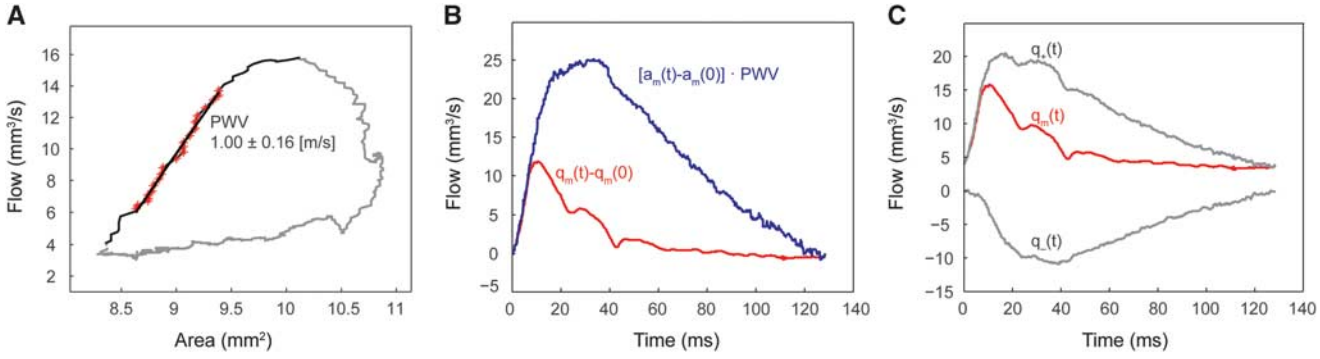

Figure 2. Decomposition of a flow waveform into its forward and reflected components. (**A**) Calculation of pulse-wave velocity (PWV) based on the change in flow versus area. (**B**) Scaled area (a_m) and flow (q_m) waveforms, after baseline subtraction. (**C**) Calculation of the forward (q_+) and reflected (q_-) waveforms using equation (1).

results from this analysis, applied to the eight mice, are presented in Table 2 and described below.

Pulse-wave velocity and reflection transit time were not statistically different between control and hypercapnic conditions. In both states, the calculated mean distance to the sites of reflection was ~5.2 mm, a position beyond the carotid bifurcation near the carotid canal at the base of the skull, and in proximity of small side branches of both the internal and external carotids.[30]

The modulus and phase of $Z_{in}(\omega)$, averaged across all mice, is plotted in Figure 3. Under both gas conditions, $|Z_{in}|$ decreased quickly over the first four harmonics. At higher harmonics, $|Z_{in}|$ changes were more gradual and a weak minimum was observed

Table 2. Calculated hemodynamic parameters

	Control (mean ± s.d.)	*Hypercapnia (mean ± s.d.)*	P	*Absolute change (mean ± s.d.)*	*% change (mean)*
PWV (m/s)	1.3 ± 0.3	1.5 ± 0.4	0.15	0.2 ± 0.3	15%
Transit time (ms)	8.0 ± 1.2	7.1 ± 0.6	0.09	0.8 ± 1.2	9%
Reflection site (mm)	5.2 ± 1.3	5.2 ± 1.2	0.9	0.1 ± 1.6	5%
Γ_t	0.57 ± 0.08	0.68 ± 0.08	0.04	0.10 ± 0.12	20%
$\lvert\Gamma(\omega = 1)\rvert$	0.62 ± 0.08	0.73 ± 0.06	0.02	0.10 ± 0.09	18%

PWV, pulse-wave velocity; Γ_t, time-domain reflection coefficient; $\lvert\Gamma(\omega = 1)\rvert$, frequency-domain reflection coefficient at first harmonic (fundamental frequency).

at the seventh harmonic. No significant difference in $|Z_{in}|$ between the two gas states was detected. The phase of Z_{in} was similar under each gas state, but a more negative phase was detected at the fundamental frequency with hypercapnia.

Reflection values calculated in the time domain, Γ_t, and frequency domain, $|\Gamma(\omega = 1)|$, were strongly correlated ($R^2 = 0.82$, mean difference ± s.d. = 0.04 ± 0.03), consistent with previous studies of human systemic reflection.[8] The frequency-domain reflection coefficient, averaged across all mice, is shown in Figure 4. Values decreased to a minimum at the fifth to sixth harmonic before rising again at higher frequencies. Interestingly, increased reflection was observed with hypercapnia, based on both definitions of reflection (Table 2).

Under both gas conditions, the onset slope of the reflected wave was significantly less than that of the forward wave. Under control conditions, the normalized slopes for the reflected and forward waves were 97 ± 22 per second versus 54 ± 23 per second ($P = 0.003$), respectively. These normalized values were not significantly different under hypercapnia. Potential sources of reduced acceleration of the reflected wave include having a distribution of distances to downstream reflection sites, a reduced reflection of high-frequency components, and a frequency-dependent PWV (wave dispersion).

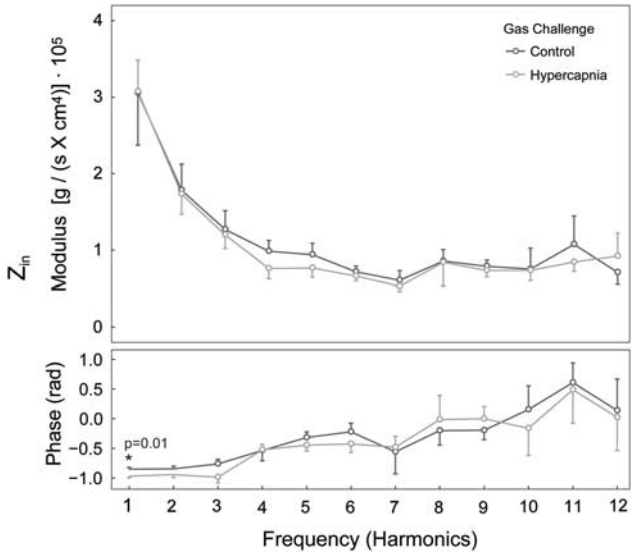

Figure 3. Input impedance measured in the left common carotid artery of mouse. Lines represent mean values obtained from eight mice under normocapnic (dark line) and hypercapnic (gray line) ventilation. For clarity, s.e. in the mouse are plotted one sided. Significant differences between normocapnic and hypercapnic values are marked by an asterisk.

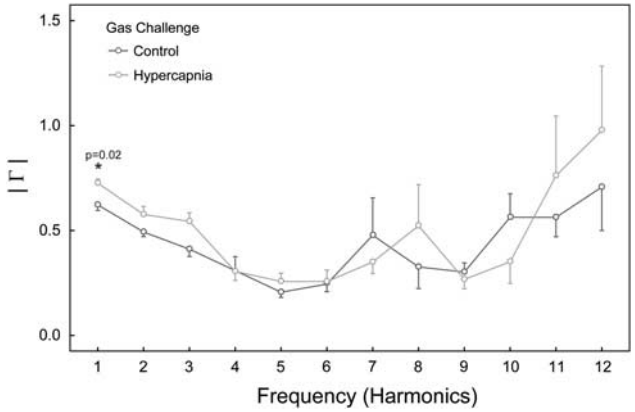

Figure 4. Modulus of the reflection coefficient measured in the left common carotid artery of mouse. Lines represent mean values obtained from eight mice under normocapnic (dark line) and hypercapnic (gray line) ventilation. For clarity, s.e. in the mean are plotted one sided. Significant differences between normocapnic and hypercapnic values are marked by an asterisk.

DISCUSSION

Vascular impedance and wave reflection in the mouse CCA were studied using noninvasive ultrasound under normocapnic and hypercapnic conditions. Compared with work using intraluminal catheters, the use of ultrasound offers significant advantages including a more natural physiological state, unencumbered by intravascular devices, and reduced morbidity associated with intervention to facilitate longitudinal assessment. Magnetic resonance imaging provides similar capabilities, enabling measurement of blood flow in large vessels[31] and also tissue perfusion.[32] Moreover, combined with hypercapnia challenges, magnetic resonance imaging techniques such as blood oxygen level-dependent imaging and arterial spin labeling can be used to assess microvascular reactivity.[22,33] However, application of magnetic resonance imaging to small animals is challenging because acquisition times are relatively long compared with the timescale of physiological changes, and achieving adequate spatial and temporal resolutions is difficult. In this regard, high-frequency ultrasound is a convenient tool that provides both anatomical and physiological data at high spatial and temporal resolutions for studies of cerebrovascular reactivity in mice.

Here, we review the findings of the present study in the context of previous work. With hypercapnia, CCA flow was found to increase by 59% over control conditions. This is comparable to previous human studies reporting an internal carotid artery (ICA) flow increase of ~50% with 5% CO2.[34] The increase in flow observed in our study can be partially attributed to a rise in heart rate (~8%); however, the balance of the increase indicates a preferential dilation of the cerebral vasculature relative to the systemic circulation. Previous studies have directly visualized cerebral vasodilation in mouse, using high energy x-ray angiography.[35] These studies varied arterial CO2 between hypocapnic and hypercapnic conditions and observed a 25% dilation of the central cerebral vessels.

The PWV values observed in the present study (1.3 ± 0.3 m/s) were generally lower than the 3 m/s reported in a previous study

of 5- to 6-month-old CD-1 mice.[36] Differences in age, anesthetic and mouse strain may explain these differences. In addition, there are differences in methodology between the two studies. Specifically, the present study used M-mode rather than color Doppler to assess cross-sectional area with greater precision. We also used total least square regression when estimating PWV to avoid bias associated with uncertainty in both the flow and area estimates. Finally, PWV is also prone to underestimation when the systolic rise of the flow and area traces is not completely free of reflected waves.[37]

Although the goal of the present study was not to measure PWV *per se*, misestimation of this parameter had the potential to bias our estimate of reflection. We evaluated this bias by extending the analytic framework of Segers *et al*,[37] and simulated the effect of PWV error on the calculated reflection magnitude. For typical values of downstream reflection (e.g., $|\Gamma(\omega)| \geq 0.2$), a 50% error in PWV resulted in just a 5% error in reflection. Intuitively, reflection estimates are less biased than PWV because of cancellation of errors in the calculated forward and backward waves, such that their ratio in the frequency domain (i.e., the reflection coefficient) is relatively preserved. It is important to note that calculations of the input impedance ($Z_{in}(\omega)$) do not assume a reflection-free period and are independent of the PWV calculation, so are not affected by PWV bias. Based on these observations, the reflection coefficient and input impedance appear to be robust parameters for the evaluation of downstream microvascular tone, even in the presence of more proximal reflections that may bias the calculation of PWV obtained using the flow-area method.

Pulse-wave velocity and transit time were not significantly affected by hypercapnia, consistent with the expectation that the biomechanics of the conduit arteries and the distance to the site of reflection would not be affected by hypercapnia-induced changes in vessel tone. The estimated position of the nearest reflection site, 5.2 ± 1.3 mm distal to the measurement site, is interesting as it places the first reflector beyond the carotid bifurcation. Moreover, because most of the mouse CCA blood flow passes through the ICA to the brain (range = 76% to 90%, $N = 3$), we speculate that the initial reflection arises from bifurcations within the ICA circulation at the level of the circle of Willis.

Impedance and reflection values for the CCA vary between species, depending on factors such as the relative tissue volumes supplied by the ICA and external carotid artery (ECA), and collateralization between the two networks.[38] This is important because the resistance per unit volume of the ECA circulation is higher than that of the intracerebral circulation, and the vasculature supplied by the ECA is less reactive to hypercapnia.[34,38] As a result, differences in flow distribution between the ECA and ICA, and the relative volumes of tissue perfused by each, will affect CCA impedance measurements. In the present study, flow through the ICA was several fold greater than that through the ECA, indicating that CCA impedance measurements should closely parallel those of the ICA in mice. Indeed, the mouse CCA impedance (Figure 3) resembled that measured in canine studies after ECA occlusion.[38] This observation that mouse CCA flow is primarily intracerebral supports the use of mouse models to study intracerebral physiology based on hemodynamic measurements from the larger and more accessible CCA.

The CCA impedance observed in this study was similar to that predicted by a three-element Windkessel model.[27] Using this model, the hypercapnic decrease in the phase of Z_{in} at low harmonics may be interpreted as an increase in total arterial compliance.[8] This subtle change, consistent with relaxed cerebrovascular tone under hypercapnia, produced a small but statistically significant increase in the reflection coefficient at the fundamental frequency. Because neither $|Z_{in}|$ nor PWV (i.e., characteristic impedance) was significantly affected by hypercapnia, this reflection change may be attributed to the change in compliance alone, demonstrating the ability of this approach to interrogate specific aspects of the mouse cerebrovasculature.

A limitation of this study was the need to combine M-mode and Doppler data acquired with the transducer in different orientations. Dual-transducer systems exist to overcome this limitation but were not available for this study.[20] However, heart rates were stable within each gas state (coefficient of variation $< 1\%$), and the measured diameter and velocity waveforms were highly reproducibility between beats (Figure 1), supporting the use of data acquired at different times.

A second limitation of this noninvasive study was the inability to calculate vascular resistance, $Z_{in}(0)$. Linearity between vessel cross-sectional area and arterial pressure has previously been demonstrated in the human carotid artery.[15] While this permitted calculation of relative changes in arterial pressure, absolute pressure remained unknown and, as a result, vascular resistance could not be calculated from the acquired ultrasound data. However, the relative vascular resistance of hypercapnia versus control conditions could be calculated ($87 \pm 12\%$), based on the relatives changes in flow and area. Furthermore, the noninvasive nature of this approach enables study of impedance in vasculature too small to instrument without affecting the physiology of interest.

A third limitation in this study was the assumption of constant PWV between the sites of measurement and reflection, used for calculation of the distance to the site of reflection. Vascular compliance depends on factors such as the ratio of elastin to collagen, the degree of muscularization, and the ratio of wall thickness to lumen diameter, which may vary along the length of a vessel.

In conclusion, we have demonstrated the use of high-frequency ultrasound for the study of cerebrovascular impedance and reflection in a cohort of mice under hypercapnia and control conditions. This approach may be applied to genetic and experimental mouse models of human pathology to improve our understanding of disrupted cerebrovascular reactivity and its response to therapy.

DISCLOSURE/CONFLICT OF INTEREST

The authors declare no conflict of interest.

ACKNOWLEDGMENTS

We thank Shoshana Spring, Sharon Portnoy, and Doreen Engelberts for their help with the blood gas analysis.

REFERENCES

1 Portegies ML, de Bruijn RF, Hofman A, Koudstaal PJ, Ikram MA. Cerebral vasomotor reactivity and risk of mortality: the Rotterdam Study. *Stroke* 2014; **45**: 42–47.
2 Hirata K, Yaginuma T, O'Rourke MF, Kawakami M. Age-related changes in carotid artery flow and pressure pulses: possible implications for cerebral microvascular disease. *Stroke* 2006; **37**: 2552–2556.
3 Prohovnik I, Hurlet-Jensen A, Adams R, De Vivo D, Pavlakis SG. Hemodynamic etiology of elevated flow velocity and stroke in sickle-cell disease. *J Cereb Blood Flow Metab* 2009; **29**: 803–810.
4 Chen CH, Hu HH, Lin YP, Chern CM, Hsu TL, Ding PY. Increased arterial wave reflection may predispose syncopal attacks. *Clin Cardiol* 2000; **23**: 825–830.
5 Czosnyka M, Smielewski P, Kirkpatrick P, Piechnik S, Laing R, Pickard JD. Continuous monitoring of cerebrovascular pressure-reactivity in head injury. *Acta Neurochir Suppl* 1998; **71**: 74–77.
6 den Abeelen AS, Lagro J, van Beek AH, Claassen JA. Impaired cerebral autoregulation and vasomotor reactivity in sporadic Alzheimer's disease. *Curr Alzheimer Res* 2014; **11**: 11–17.
7 Murgo JP, Westerhof N, Giolma JP, Altobelli SA. Aortic input impedance in normal man: relationship to pressure wave forms. *Circulation* 1980; **62**: 105–116.
8 Segers P, Rietzschel ER, De Buyzere ML, Vermeersch SJ, De Bacquer D, Van Bortel LM *et al*. Noninvasive (input) impedance, pulse wave velocity, and wave reflection in healthy middle-aged men and women. *Hypertension* 2007; **49**: 1248–1255.

9 Huez S, Brimioulle S, Naeije R, Vachiery JL. Feasibility of routine pulmonary arterial impedance measurements in pulmonary hypertension. *Chest* 2004; **125**: 2121–2128.
10 Hunter KS, Lee PF, Lanning CJ, Ivy DD, Kirby KS, Claussen LR *et al.* Pulmonary vascular input impedance is a combined measure of pulmonary vascular resistance and stiffness and predicts clinical outcomes better than pulmonary vascular resistance alone in pediatric patients with pulmonary hypertension. *Am Heart J* 2008; **155**: 166–174.
11 Morales Rosello J, Hervas Marin D, Fillol Crespo M, Perales Marin A. Doppler changes in the vertebral, middle cerebral, and umbilical arteries in fetuses delivered after 34 weeks: relationship to severity of growth restriction. *Prenat Diagn* 2012; **32**: 960–967.
12 Wong KS, Li H, Chan YL, Ahuja A, Lam WW, Wong A *et al.* Use of transcranial Doppler ultrasound to predict outcome in patients with intracranial large-artery occlusive disease. *Stroke* 2000; **31**: 2641–2647.
13 Kelly R, Fitchett D. Noninvasive determination of aortic input impedance and external left ventricular power output: a validation and repeatability study of a new technique. *J Am Coll Cardiol* 1992; **20**: 952–963.
14 Mitchell GF, Vita JA, Larson MG, Parise H, Keyes MJ, Warner E *et al.* Cross-sectional relations of peripheral microvascular function, cardiovascular disease risk factors, and aortic stiffness: the Framingham Heart Study. *Circulation* 2005; **112**: 3722–3728.
15 Sugawara M, Niki K, Furuhata H, Ohnishi S, Suzuki S. Relationship between the pressure and diameter of the carotid artery in humans. *Heart Vessels.* 2000; **15**: 49–51.
16 Hebert F, Grand'maison M, Ho MK, Lerch JP, Hamel E, Bedell BJ. Cortical atrophy and hypoperfusion in a transgenic mouse model of Alzheimer's disease. *Neurobiol Aging* 2013; **34**: 1644–1652.
17 Greaves DR, Fraser P, Vidal MA, Hedges MJ, Ropers D, Luzzatto L *et al.* A transgenic mouse model of sickle cell disorder. *Nature* 1990; **343**: 183–185.
18 Ong PK, Meays D, Frangos JA, Carvalho LJ. A chronic scheme of cranial window preparation to study pial vascular reactivity in murine cerebral malaria. *Microcirculation* 2013; **20**: 394–404.
19 Reddy AK, Taffet GE, Madala S, Michael LH, Entman ML, Hartley CJ. Noninvasive blood pressure measurement in mice using pulsed Doppler ultrasound. *Ultrasound Med Biol* 2003; **29**: 379–385.
20 Reddy AK, Madala S, Jones AD, Caro WA, Eberth JF, Pham TT *et al.* Multichannel pulsed Doppler signal processing for vascular measurements in mice. *Ultrasound Med Biol* 2009; **35**: 2042–2054.
21 Foster FS, Mehi J, Lukacs M, Hirson D, White C, Chaggares C *et al.* A new 15-50 MHz array-based micro-ultrasound scanner for preclinical imaging. *Ultrasound Med Biol* 2009; **35**: 1700–1708.
22 Kassner A, Winter JD, Poublanc J, Mikulis DJ, Crawley AP. Blood-oxygen level dependent MRI measures of cerebrovascular reactivity using a controlled respiratory challenge: reproducibility and gender differences. *J Magn Reson Imaging* 2010; **31**: 298–304.
23 Boese JM, Bock M, Schoenberg SO, Schad LR. Estimation of aortic compliance using magnetic resonance pulse wave velocity measurement. *Phys Med Biol* 2000; **45**: 1703–1713.
24 Khir AW, O'Brien A, Gibbs JS, Parker KH. Determination of wave speed and wave separation in the arteries. *J Biomech* 2001; **34**: 1145–1155.
25 Vulliemoz S, Stergiopulos N, Meuli R. Estimation of local aortic elastic properties with MRI. *Magn Reson Med* 2002; **47**: 649–654.
26 Glaister P. Least squares revisited. *Math Gazette* 2001; **85**, S 104–107.
27 Westerhof N, Lankhaar JW, Westerhof BE. The arterial Windkessel. *Med Biol Eng Comput* 2009; **47**: 131–141.
28 Laxminarayan S. The calculation of forward and backward waves in the arterial system. *Med Biol Eng Comput* 1979; **17**: 130.
29 Li JK. Time domain resolution of forward and reflected waves in the aorta. *IEEE Trans Biomed Eng* 1986; **33**: 783–785.
30 Howles GP, Ghaghada KB, Qi Y, Mukundan S, Jr, Johnson GA. High-resolution magnetic resonance angiography in the mouse using a nanoparticle blood-pool contrast agent. *Magn Reson Med* 2009; **62**: 1447–1456.
31 Lotz J, Meier C, Leppert A, Galanski M. Cardiovascular flow measurement with phase-contrast MR imaging: basic facts and implementation.*Radiographics* 2002; **22**: 651–671.
32 Forbes ML, Hendrich KS, Kochanek PM, Williams DS, Schiding JK, Wisniewski SR *et al.* Assessment of cerebral blood flow and CO2 reactivity after controlled cortical impact by perfusion magnetic resonance imaging using arterial spin-labeling in rats. *J Cereb Blood Flow Metab* 1997; **17**: 865–874.
33 Barbier EL, Silva AC, Kim SG, Koretsky AP. Perfusion imaging using dynamic arterial spin labeling (DASL). *Magn Reson Med* 2001; **45**: 1021–1029.
34 Sato K, Sadamoto T, Hirasawa A, Oue A, Subudhi AW, Miyazawa T *et al.* Differential blood flow responses to CO(2) in human internal and external carotid and vertebral arteries. *J Physiol* 2012; **590**: 3277–3290.
35 Kidoguchi K, Tamaki M, Mizobe T, Koyama J, Kondoh T, Kohmura E *et al. In vivo* X-ray angiography in the mouse brain using synchrotron radiation. *Stroke* 2006; **37**: 1856–1861.
36 Williams R, Needles A, Cherin E, Zhou YQ, Henkelman RM, Adamson SL *et al.* Noninvasive ultrasonic measurement of regional and local pulse-wave velocity in mice. *Ultrasound Med Biol* 2007; **33**: 1368–1375.
37 Segers P, Swillens A, Taelman L, Vierendeels J. Wave reflection leads to over- and underestimation of local wave speed by the PU- and QA-loop methods: theoretical basis and solution to the problem. *Physiol Meas* 2014; **35**: 847–861.
38 Taylor DE, Tukmachi ES. Contribution of internal and external carotid beds to common carotid artery input impedance in the dog. *Q J Exp Physiol* 1985; **70**: 177–187.